International Journal of Mass Spectrometry 306 (2011) 27–36

Contents lists available at ScienceDirect

International Journal of Mass Spectrometry

journal homepage: www.elsevier.com/locate/ijms

Unimolecular reactivity upon collision of uracil–Ca^{2+} complexes in the gas phase: Comparison with uracil–M^+ (M = H, alkali metals) and uracil–M^{2+} (M = Cu, Pb) systems

Cristina Trujillo [a], Al Mokhtar Lamsabhi [a], Otilia Mó [a], Manuel Yáñez [a], Jean-Yves Salpin [b,c,*]

[a] Departamento de Química, Módulo 13, Universidad Autónoma de Madrid, Cantoblanco, Campus de Excelencia UAM-CSIC, 28049 Madrid, Spain
[b] Université d'Evry Val d'Essonne – Laboratoire Analyse et Modélisation pour la Biologie et l'Environnement (LAMBE) – Bâtiment Maupertuis, Boulevard François Mitterrand, 91025 Evry, France
[c] CNRS – UMR 8587, France

ARTICLE INFO

Article history:
Received 17 March 2011
Received in revised form 27 May 2011
Accepted 29 May 2011
Available online 6 June 2011

Keywords:
Nanoelectrospray/mass spectrometry
DFT calculations
Unimolecular reactivity upon collision
Calcium
Uracil
Potential energy surfaces

ABSTRACT

The stability against collisional dissociation of [uracil–Ca]$^{2+}$ complexes has been investigated by combining nanoelectrospray ionization/mass spectrometry techniques and B3LYP/6-311++G(3df,2p)//B3LYP/6-31+G(d,p) density functional theory (DFT) calculations. The reactivity upon collision seems to be dominated by Coulomb explosion processes, since the most intense peaks in the MS/MS spectra correspond to singly-charged species ($CaOH^+$ and $[C_4,H_3,N_2,O]^+$). Nevertheless, additional peaks corresponding to the loss of neutral species, namely [H,N,C,O] and H_2O have been also detected. A systematic study of the CID spectra obtained with different labeled species, namely, 2-^{13}C-uracil, 3-^{15}N-uracil and 2-^{13}C-1,3-$^{15}N_2$-uracil, concludes unambiguously that the loss of [H,N,C,O] involves exclusively atoms C2 and N3. Suitable mechanisms for these fragmentation processes are proposed through a theoretical survey of the corresponding potential energy surface. A comparison between these results and those reported for two other metal dications, namely Cu^{2+} and Pb^{2+}, as well as for protonated uracil and uracil–M^+ (M = Li, Na, K) complexes denotes the existence of significant differences and interesting similarities, among the various systems.

1. Introduction

The interaction of different DNA bases with metal ions has received a lot of attention along the years. Most of these studies were focused on the interactions with singly-charged metal ions, both alkali metal ions and transition metal ions [1–14]. More recently, many publications reported studies in which the metal ion interacting with the base is a doubly-charged species, in particular alkaline-earth metal dications [6,7,15–21], but also transition metal dications such as Cu^{2+}, Ni^{2+} or Zn^{2+} [7,11,22,23]. As a consequence, a lot of information has been gathered mainly on the structure of the corresponding complexes and on the effects of the metal ion on the geometry of the base or in its capacity to form pairs with other bases [7,15,22]. However, the information about the unimolecular reactivity of these complexes is much scarcer and fragmentary. One of the important reasons behind this lack of information is the fact that many of the doubly-charged complexes formed by the association of the base with the metal dication are not stable species in the gas phase, and most of them typically decompose by losing a proton of the nucleobase [24]. We have shown for different systems of biochemical interest, such as urea [25,26], thiourea [26,27], selenourea [28], glycine [29], that this is not the case when the doubly-charged metal ion is Ca^{2+}, because when this ion interacts with all the aforementioned systems, the deprotonation process turns out to be endothermic and the doubly-charged complex is stable both with respect to the loss of a proton or to an alternative Coulomb explosion yielding Ca^+ [30].

Due to the enormous relevance of uracil as a biochemical system, it has been the object of many different studies, and notably those dealing with its gas-phase interactions with [Cu^{2+}] [31–33] and [Pb^{2+}] [34,35]. Since Ca^{2+} is ubiquitous in the biochemical media, we thought that it was of interest to extend the previous studies to Ca^{2+} ions, with the aim of establishing whether the reactivity depends strongly on the nature of the metal dication or if on the contrary, all reactions exhibit similar patterns, being the critical factor the fact that one of the reactants has a large positive charge which strongly polarizes the base.

For this purpose, the gas-phase interactions of Ca^{2+} with uracil have been investigated by means of nanoelectrospray

* Corresponding author at: Université d'Evry Val d'Essonne – Laboratoire Analyse et Modélisation pour la Biologie et l'Environnement (LAMBE) – Bâtiment Maupertuis, Boulevard François Mitterrand, 91025 Evry, France. Tel.: +33 1 69 47 76 44; fax: +33 1 69 47 76 55.
E-mail address: jean-yves.salpin@univ-evry.fr (J.-Y. Salpin).

1387-3806/$ – see front matter © 2011 Elsevier B.V. All rights reserved.
doi:10.1016/j.ijms.2011.05.018

ionization/mass spectrometry techniques, whose results were then analyzed and interpreted by exploring the topology of the corresponding potential energy surface by means of accurate density functional theory calculations. This allowed us to compare the behavior of this alkaline-earth dication with that of two other doubly-charged metal ions, namely Cu^{2+} and Pb^{2+}, which are also biochemically relevant [36–39], although for different reasons, since Ca and Cu can be considered as oligoelements while Pb is a well-known poison [40]. This comparison can provide new insights about the gas-phase interaction of uracil with metal dications.

2. Experimental and computational details

2.1. Experimental

Electrospray MS/MS mass spectra were recorded on a QSTAR PULSAR i (Applied Biosystems/MDS Sciex) hybrid instrument (QqTOF) fitted with a nanospray source. Typically, 6 μL of a 1:1 aqueous mixture of calcium chloride and uracil (10^{-4} mol L^{-1}) were nanosprayed (20–50 nL/min) using borosilicate emitters (Proxeon). The sample was ionized using an 800–900 V nanospray needle voltage and the lowest possible nebulizing gas pressure (tens of millibars). The declustering potential DP (also referred to as "cone voltage" in other devices), defined as the difference in potentials between the orifice plate and the skimmer (grounded), ranged from 0 to 120 V. The operating pressure of the curtain gas (N_2), which prevents air or solvent from entering the analyzer region, was adjusted to 0.7 bar by means of pressure sensors, as a fraction of the N_2 inlet pressure. To improve ion transmission and subsequent sensitivity during the experiments, the collision gas (CAD, N_2) was present at all times for collisional focusing in both the Q0 (ion guide preceding the quadrupole Q1 and located just after the skimmer) and Q2 (collision cell) sectors.

For MS/MS spectra, complexes of interest were mass-selected using Q1, and allowed to collide with nitrogen as collision gas in the second quadrupole (Q2), the resulting product ions being analyzed by the time-of-flight (TOF) after orthogonal injection. Furthermore, MS/MS spectra were systematically recorded at various collision energies ranging from 7 eV to 16 eV in the laboratory frame (the collision energy is given by the difference between the potentials of Q0 and Q2). The CAD parameter, which controls the amount of N_2 introduced into Q2, was set to its minimum value in order to limit multiple ion–molecule collisions. All experiments were performed in 100% water purified with a Milli-Q water purification system. All nucleobases but 3-^{15}N-uracil (see Acknowledgments) and calcium chloride were purchased from Aldrich (St Quentin-Fallavier, France) and were used without further purification.

2.2. Computational details

Density functional theory (DFT) calculations were carried out using the B3LYP hybrid functional, as implemented in the Gaussian 03 suite of programs [41]. B3LYP combines the nonlocal correlation function of Lee et al. [42], with Becke's three-parameter non local hybrid exchange functional [43].

We have chosen the hybrid functional B3LYP because, in a previous assessment [44], it has been shown to provide reliable results when dealing with Ca^{2+} interactions. The different structures have been first optimized with a dp-polarized 6-31+G(d,p) basis set expansion, which includes diffuse functions on the heavy atoms. Harmonic vibrational frequencies were computed at the same level in order to estimate the corresponding zero-point vibrational energy (ZPVE) corrections (scaled by 0.986 [45]) and to classify the stationary points of the PES either as local minima or transition states (TS). Intrinsic reaction coordinate (IRC) calculations were carried out to ascertain the connection between TS and local minima. In order to ensure the reliability of our relative energies when analyzing the topology of the corresponding potential energy surface (PES), the final energy of each of the stationary points was refined by single-point calculations using the much larger and flexible 6-311+G(3df,2p) basis. It should be mentioned that this level of theory predicts as the most stable structure of uracil–Li^+ complexes the structure in which the metal ion binds the carbonyl oxygen at position 4 (Scheme 1), in fairly good agreement with recent IRMPD results which suggest this to be the most stable structure in complexes between uracil and hydrated-Li^+ [12]. This good agreement can be taken as an indirect assessment of the level of theory used in this work.

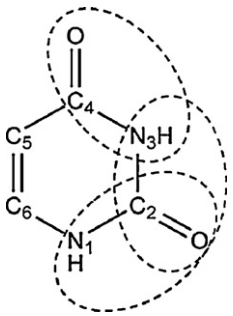

Scheme 1. Possibilities for the loss of [H,N,C,O] fragment.

The bonding characteristics were investigated by means of the atoms in molecules (AIM) theory [46,47], in particular through the analysis of the molecular graphs and of the energy density:

$$h(\vec{r}) = v(\vec{r}) + g(\vec{r}) \quad (1)$$

where $v(\vec{r})$ and $g(\vec{r})$ are the local densities of the kinetic energies, respectively. The regions in which this magnitude is negative or positive correspond to areas in which the electron density is built up or depleted, respectively, so that the former can be associated with covalent interactions, whereas the latter are typically associated with closed-shell interactions, as in ionic bonds or hydrogen bonds. The molecular graphs are defined by the ensemble of the bond critical points and the bond paths. The corresponding density energy plots have been obtained by means of the AIMPAC series of programs [48].

3. Results and discussion

3.1. Mass spectrometry

A typical nanoelectrospray spectrum recorded at DP = 20 V for a 1:1 aqueous mixture of $CaCl_2$/uracil (10^{-4} M) is given in Fig. 1a.

Several series of ions are observed and use of labeled uracils allows an easy identification of the ions involving uracil. In the low-mass range, hydrated Ca^{2+} ions $[Ca(H_2O)_i]^{2+}$ (i = 1–3) are detected at m/z 29.00, 37.99 and 46.99, respectively. Their intensity is particularly high when the DP parameter is set to 0 V and then quickly drops off when the declustering potential is increased. Calcium hydroxide (m/z 56.97) is also detected but in weak abundance over the all range of DP values. This spectrum therefore differs significantly from the electrospray spectra obtained with Cu(II) and Pb(II) salts, which exhibit intense metal hydroxide MOH^+ ions [33,34]. The electrospray spectrum is presently dominated by protonated uracil (m/z 113.03). This was rather expected given the rather high proton affinity of this nucleobase compared to that of water [49]. Like for $[Pb^{2+}]$ [34,35] and $[Cu^{2+}]$ [33], singly-charged complexes of the type $[M(uracil)_m–H]^+$ (m = 1–3) are detected at m/z 150.99, 263.03 and 375.07. In addition, doubly-charged com-

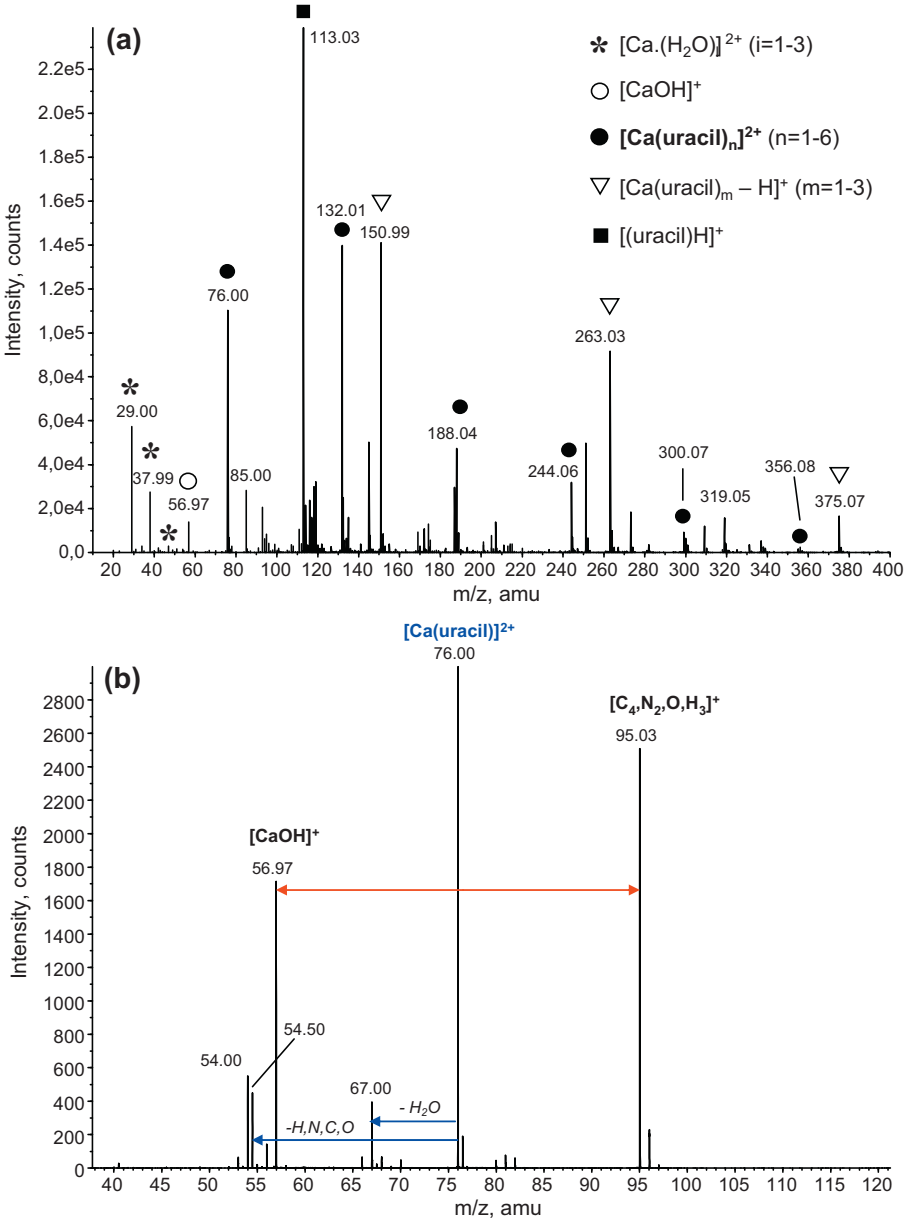

Fig. 1. (a) Positive-ion nanospray spectrum of an aqueous mixture of calcium chloride and uracil (1:1 ratio, 10^{-4} M) and (b) low-energy MS/MS spectrum of the $[Ca(uracil)]^{2+}$ complex (m/z 76.00) recorded at a collision energy of 12 eV (laboratory frame).

plexes of general formula $[Ca(uracil)_n]^{2+}$ (n = 1–6) are also observed with a significant intensity at m/z 76.00 and 132.01, 188.04, 244.06, 300.07 and 356.08. A hydrated $[Ca(uracil)\cdot H_2O]^{2+}$ complex is also detected at m/z 85.00. Interaction of metal dications with organic ligands L generally results in the detection on electrospray spectra of a series of $[ML_n]^{2+}$ complexes ($n \geq 1$) [50–60], but the smallest species $[ML]^{2+}$ (n = 1) is often not observed, especially for metals having a high second ionization energy such as copper or lead. Consistently, in the case of the Cu^{2+}/uracil and Pb^{2+}/uracil systems, no $[M(uracil)]^{2+}$ ions were observed, but we did neither detect higher homologues in the case of copper [33]. Note that this was also the case in a recent electrospray study of the Ca^{2+}/uracil system [19], indicating that the geometry of the ESI interface may have a strong influence on the observation of these species.

Increasing the DP value results in the fast removal of the doubly-charged complexes by "in source" fragmentation processes. At high DP values, the most abundant species detected are protonated uracil and singly-charged $[Ca(uracil)_m–H]^+$ (m = 1,2) complexes. Consequently, we opted for a low DP value to record the MS/MS spectra of the various doubly charged species.

MS/MS spectra of all the $[Ca(uracil)_n]^{2+}$ complexes have been recorded (not shown). For $n \geq 2$, two competitive processes are systematically observed: (1) elimination of neutral uracil leading to the $[Ca(uracil)_{n-1}]^{2+}$ ion and (2) an interligand proton transfer followed by charge separation driven by Coulomb explosion, giving rise to the $[Ca(uracil)_{n-1}–H]^+$ complex and protonated uracil (m/z 113.03). In turn, these newly-formed complexes may expel one uracil unit. Loss of intact uracil dominates for n = 4–5 while the interligand proton transfer becomes prominent for n = 2–3. In order to rationalize the behavior upon collision of the doubly-charged complexes, two parameters n_{crit} and n_{min} were introduced [57]. The first one, namely n_{crit}, is defined as the largest value of n at and below which $M^{2+}(L)_n$ decomposes not solely by neutral evaporation but also via charge (electron and/or proton) transfer as well. Our MS/MS spectra show that for Ca^{2+} ions and uracil, the n_{crit} parameter is at least equal to 5. In spite of extensive tuning, the

$[Ca(uracil)_6]^{2+}$ (m/z 356.08) could be detected only in very small amounts, so that its MS/MS spectrum could not be recorded. The second parameter n_{min} is defined as the minimum number of ligands for which $M^{2+}(L)_n$ complexes, under CID conditions, remain stable against spontaneous dissociative electron transfer or proton transfer reactions. A value of 0 for n_{min} may be presently attributed as bare Ca^{2+} ions are detected when recording the MS/MS spectrum of the $[Ca(uracil)]^{2+}$ complex at high collision energy, though in very small abundance.

Globally, the dissociation upon collision of this latter complex markedly differs from its higher homologues since its MS/MS spectrum (Fig. 1b) is characterized by elimination of water (m/z 67.00) and of a 43 Da [H,N,C,O] moiety (m/z 54.50). This latter process is the only dissociation channel observed for the $[Ca(uracil)–H]^+$ complex (not shown), and is also observed for both $[Pb(uracil)–H]^+$ and $[Cu(uracil)–H]^+$ complexes [33,34]. One may reasonably assume that elimination of 43 Da without extensive rearrangement requires adjacent atoms to be expelled. In that particular case, isocyanic (H–N=C=O) acid should be eliminated rather than cyanic acid (HO–C≡N). According to Scheme 1, three possibilities may be envisaged for the loss of [H,N,C,O]: HN3C2O, HN1C2O and HN3C4O.

Consequently, the only way to establish the connectivity of the fragments without ambiguity is by using appropriate labeled species. For this purpose, besides the non-labeled complex (m/z 76.00) the labeled complexes generated with 2-^{13}C-uracil (m/z 76.52), 2-^{13}C–1,3-$^{15}N_2$ uracil (m/z 77.50) and 3-^{15}N-uracil (m/z 76.50) were studied. A summary of the labeled products ions observed by CID in each case is given in Table 1.

When using either 2-^{13}C- or 3-^{15}N-uracil species, a loss 44 Da is observed (m/z 54.5). This product ion is shifted at m/z 54.99 (elimination of 45 Da) when 2-^{13}C–1,3-$^{15}N_2$ uracil is considered. Consequently, these experiments clearly demonstrate that the loss of HNCO involves exclusively the elimination of the C2 and N3 atoms and that the HN3C2O fragment should be expelled. This fragmentation process is therefore similar to what is observed for $[M(uracil)–H]^+$ complexes (M = Cu, Pb, Ca). It is worth mentioning that the same loss was also observed in collision induced dissociation of protonated uracil, although in this particular case a 10% and 3% of HN1C2O and HN3C4O, respectively, were also detected [61]. The loss of HNCO, although without identifying the atoms actually eliminated, was also detected onto the photodissociation spectrum of the $[Mg(uracil)]^+$ gaseous complexes [62], as well as for uracil in photoionization mass spectrometry studies at 20 eV photon excitation energy [63], electron ionization experiments carried out at 70 eV [64] and 20 eV electron ionization energies [65], and more recently also in proton impact experiments [66]. We will come back to these results in the last section of this paper.

Apart from the loss of [H,N,C,O], the MS/MS spectrum of the $[Ca(uracil)]^{2+}$ complex is dominated by a charge separation process giving rise to $[Ca,O,H]^+$ (m/z 56.97) and a $[C_4,N_2,O,H_3]^+$ species detected at m/z 95.03. The former presumably corresponds to calcium hydroxide (*vide supra*). The latter peak is logically shifted as labeled uracils are used (Table 1). In order to have more information about the structure of this product ion, we recorded its CID spectrum. To this end, this ion was generated in sufficient abundance by in source fragmentation. It certainly mostly arose from the doubly charged complex as loss of water from protonated uracil is only a very minor process. Three peaks are observed and correspond to the loss of 27, 28 and 42 Da. Again, use of labeled uracils provides useful insights about the structure of this product ion. First, elimination of 28 Da is always observed, suggesting that this process should correspond to elimination of carbon monoxide. Interestingly, as the loss of 28 Da is still observed with 2-^{13}C-uracil, the CO moiety would involve the C4 atom. The elimination of 27 Da is observed for all uracils but 2-^{13}C–$^{15}N_2$-uracil. For this particular reactant, only a loss of 28 Da is observed and the elimination of [H,C,N] and CO therefore cannot be distinguished. Consequently, the [H,C,N] fragment involves the N1 atom. It is worth noting that the m/z 53 ion is systematically detected regardless of the uracil considered. Therefore, this particular fragmentation should rather be associated with the elimination of a $[C,H_2,N_2]$ unit instead of a ketene molecule. In summary, the fragmentation pattern of complexes involving divalent metals is much richer than the one observed with alkali metals, since a recent threshold collision induced dissociation study has shown that M^+–uracil complexes (M = Li, Na, K) react solely by loss of the intact uracil [2]. To conclude this section, note that one can also observe on Fig. 1b a peak at m/z 54.00, but its attribution is still unclear.

3.2. Computational study

In order to rationalize the experimental findings, we carried out a theoretical study that will enable us to explore the potential energy surfaces associated with the $[Ca(uracil)]^{2+}$ ion fragmentation processes. The energies of the corresponding stationary minima and transitions states are reported in Table S1 of Supporting Information. Recently, we have shown [67] that structures **1**, **4**, **2b** and **5b** (see Fig. 2) are the most probable structures that could be involved in the dissociation of this complex.

For the sake of consistency we have adopted the same numbering for the complexes as used in Ref. [67]. It should be reminded that these structures are connected between each other through transition states which involve activation energies much lower than the entrance channel. Therefore all of them are suitable initial structures for the $[Ca(uracil)]^{2+}$ fragmentation processes. It is worth noting that the most stable neutral structure of uracil is the diketone form instead of the dienol structure [68]. The direct interaction of Ca^{2+} occurs mainly on the oxygen which occupies position 4, and leads to form **4**, with a binding energy of about 438 kJ mol^{-1}, and on the oxygen at position 2 yielding complex **1**, the binding energy of the metal being 397 kJ mol^{-1}. Minima **5b** and **2b**, which are the most stable ones, are the result of a 1,3-hydrogen transfer from the nearby nitrogen to the oxygen atom at position 2 or 4 in the structure **4** or **1**, respectively. As mentioned above, these isomers will be taken as the starting point for the fragmentation mechanisms proposed. A fifth structure, namely complex **8** was added to the previous ones, because this π-type complexes were found to play a significant role in the reactions between uracil and other metal dications [33], and as we shall show in forthcoming sections, also contributes significantly to the reactivity of uracil with Ca^{2+}.

Two kinds of fragmentations of $[uracil–Ca]^{2+}$ complexes have been observed in the MS/MS spectra, those corresponding to Coulomb explosions leading to singly-charged species like $[Ca,O,H]^+$ and $[C_4,N_2,O,H_3]^+$ and those corresponding to the loss of a neutral moiety which yield doubly-charged product ions such as $[Ca,C_4,H_2,O,N_2]^{2+}$ and $[Ca,C_3,H_3,O,N]^{2+}$. For the sake of clarity, we will discuss each of these fragmentation mechanisms in separate sections.

3.2.1. Coulomb explosions yielding $[Ca,O,H]^+$ and $[C_4,N_2,O,H_3]^+$

As indicated in previous sections the two most intense peaks in the MS/MS spectrum are detected at m/z 56.97 and 95.03, and correspond to $[Ca,O,H]^+$ and $[C_4,N_2,O,H_3]^+$ monocations, respectively. All the four local minima (**1**, **4**, **2b** and **5b**) mentioned in the previous section can be, in principle, good precursors for the formation of $[CaOH]^+$ since, in all of them, the dication is attached to an oxygen atom. A simple hydrogen transfer from the nearby NH or CH groups would then yield a CaOH arrangement and the subsequent formation of $[CaOH]^+$. However, the mechanisms depend on the nature of the starting isomer. As shown in Fig. 3, two different mechanisms originating from the adduct **4**

Table 1
Product ions observed for the $[Ca(uracil)]^{2+}$ complex and for the m/z 95 ion, when using various labeled uracils.

Uracil	Precursor ion	Product ions			
	$[Ca(uracil)]^{2+}$	$[Ca,C_3,H_3,O,N]^{2+}$		$[C_4,H_3,N_2,O]^+$	
Not labeled	*m/z* 76.00	*m/z* 54.50	–[H,N,C,O]	*m/z* 95.03	–[Ca,O,H]$^+$
2-^{13}C	*m/z* 76.52	*m/z* 54.51	–[H,N,^{13}C,O]	*m/z* 96.04	–[Ca,O,H]$^+$
3-^{15}N	*m/z* 76.50	*m/z* 54.50	–[H,^{15}N,C,O]	*m/z* 96.03	–[Ca,O,H]$^+$
2-^{13}C–1,3-$^{15}N_2$	*m/z* 77.50	*m/z* 54.99	–[H,^{15}N,^{13}C,O]	*m/z* 98.02	–[Ca,O,H]$^+$

Uracil	Precursor ion	Product ions					
	$[C_4,N_2,O,H_3]^+$	$[C_3,H_2,N,O]^+$		$[C_3,H_3,N_2]^+$		$[C_3,H,O]^+$	
Not labeled	*m/z* 95.03	*m/z* 68.02	–[H,C,N]	*m/z* 67.02	–CO	*m/z* 53.00	–[C,H$_2$,N$_2$]
2-^{13}C	*m/z* 96.04	*m/z* 69.02	–[H,C,N]	*m/z* 68.03	–CO	*m/z* 53.00	–[^{13}C,H$_2$,N$_2$]
3-^{15}N	*m/z* 96.03	*m/z* 69.02	–[H,C,N]	*m/z* 68.03	–CO	*m/z* 53.00	–[C,H$_2$,^{15}N,N]
2-^{13}C–1,3-$^{15}N_2$	*m/z* 98.02	*m/z* 70.03	–[H,C,^{15}N]	*m/z* 70.03	–CO	*m/z* 53.00	–[^{13}C,H$_2$,^{15}N$_2$]

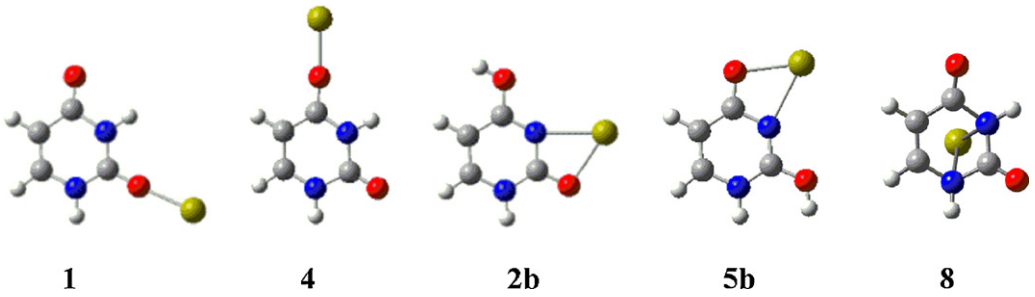

Fig. 2. B3LYP/6-31+G(d,p) geometries of the lowest energy structures of $[Ca(uracil)]^{2+}$ complexes.

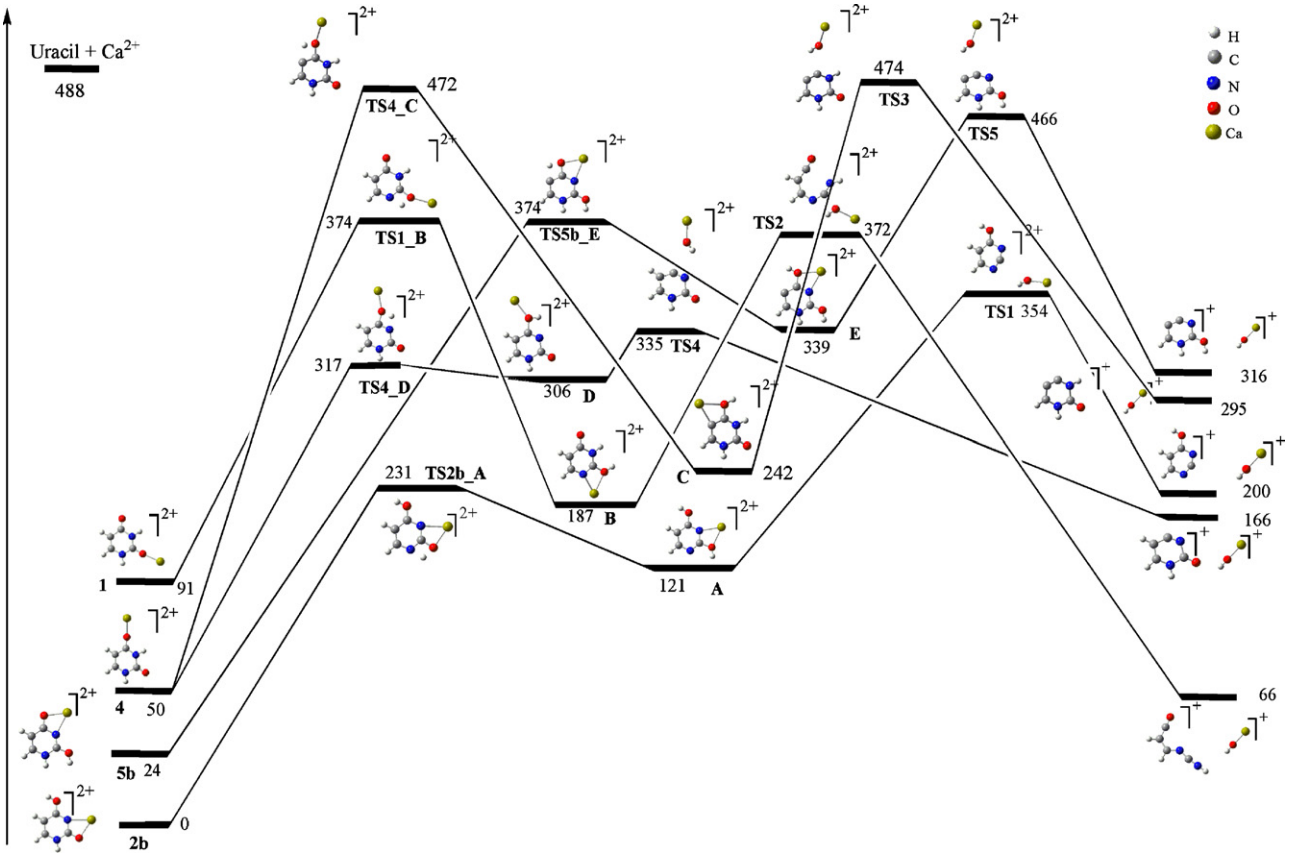

Fig. 3. Potential energy profile corresponding to the Coulomb explosions yielding $[CaOH]^+$ and with origin in local minima **1**, **4**, **5b** and the global minimum **2b**. Relative energies are in kJ mol^{-1}.

are possible depending on the hydrogen involved in the 1,3-H shift (the C5H or the N3H).

As it could be easily anticipated the latter is the most favorable one, due to the much larger intrinsic acidity of the N3H group. This 1,3-H shift leads to the intermediate **D**, which subsequently dissociates into $[CaOH]^+$ and a cyclic $CHCHNHC(O)NC^+$ structure. Note that the corresponding $NC–CH{=}CH–NH–CO^+$ acyclic ion is 11 kJ mol^{-1} higher in energy than the cyclic one shown in Fig. 3. The 1,3-H shift from the C5H group can then be discarded since the formation of the intermediate **C** involves an activation barrier (472 kJ mol^{-1}) which is very close in energy to the entrance channel.

In principle, two mechanisms with origin in form **1** could also be possible, but in order not to overload Fig. 3, only the most favorable is shown. This mechanism involves a 1,3 H shift from N1H rather than from N3H. It is well established that of the two NH groups present in uracil, N1H is the most acidic one [69], and this situation does not change when forming complexes with Ca^{2+} [67]. This hydrogen shift leads to the formation of structure **B**, which eventually dissociates yielding a very stable $OCCHCHNCNH^+$ open-chain monocation.

Alternative processes yielding $[CaOH]^+$ could also involve the enolic complexes **2b** and **5b**. The most favorable one from a thermodynamic viewpoint would have its origin in the global minimum **2b** and would imply two steps. In the first one, the N1H hydrogen migrates towards the CO group through a rather low activation barrier (231 kJ mol^{-1}). Then, the intermediate formed (**A**) would undergo a Coulomb explosion yielding $[CaOH]^+$ and the second more stable cyclic $[C_4,N_2,O,H_3]^+$ cation, through a reasonably small barrier.

The mechanism involving **5b** can be also discarded. Although the energy barrier connecting **5b** to the intermediate **E** is not too high, the one associated with the simultaneous cleavage of the C–O and N–Ca bonds in structure **E** is also very close in energy to the entrance channel (466 kJ mol^{-1}).

In summary, the fragmentation of the $[uracil–Ca]^{2+}$ complex through the charge separation process yielding $[CaOH]^+$ and $[C_4,N_2,O,H_3]^+$ may have its origin in three different structures, namely **2b**, **1** and **4**, through appropriate 1,3-H shifts. These three processes are thermodynamically allowed, and the barriers associated with the limiting step for each process are rather similar (335, 354 and 372 kJ mol^{-1}). This suggests that the loss of $[CaOH]^+$ might lead to the formation of three different $[C_4,N_2,O,H_3]^+$ isomers, two cyclic ones and one (the most stable) with an aliphatic open-chain structure. Note however that the formation of the acyclic form is consistent with the MS/MS spectrum of the *m*/*z* 95.03 ion, which, as shown before, is characterized by elimination of C(4)O, [H,C,N(1)] and $[C(2),H_2,N_2]$ subunits. Furthermore, this product would be also entropically favored with respect to the two cyclic isomers.

3.2.2. Mechanisms associated with neutral losses

The two peaks observed in the MS/MS spectrum at *m*/*z* 67.00 and *m*/*z* 54.50 corresponds to the loss of H_2O and [H,N,C,O], respectively. As mentioned in Section 3.1, the use of appropriate labeled species demonstrates that the loss of [H,N,C,O] involves specifically C2 and N3. Elimination of [H,N,C,O] was also observed on the MS/MS spectra of the $[M(uracil)–H]^+$ complexes (M = Cu [33] or Pb [34]), and interestingly involves the same atoms. The question that needs to be addressed now is what is the mechanism leading to this specific loss and what is the more likely structure of the [H,N,C,O] fragment produced. Our calculations show that isocyanic acid (H–N=C=O) is more stable by about 115 kJ mol^{-1} than cyanic acid (HO–C≡N), but in principle, as we shall discuss later, both forms should be experimentally accessible.

Although all possible mechanisms leading to the formation [H,N,C,O] and H_2O from the four most stable $[uracil–Ca]^{2+}$ complexes have been examined, we only present in Fig. 4 those involving the lowest activation barriers.

This immediately discards **1**, **4** and **2b** as starting structures, for which multiple intermediate steps characterized by very high activation barriers are required. However, we have also included in our survey the conventional π complex **8**, because this kind of complexes was found to play a fundamental role in the reactivity of uracil with other metal dications [33]. In complex **8**, Ca^{2+} interacts simultaneously with the N1 and N3 lone pairs. Although this structure is much higher in energy (about 281 kJ mol^{-1} less stable than structures **2b** and **5b**), it can play an important role in the collision induced dissociation of the $[uracil–Ca]^{2+}$ ion, because its formation induces important distortions of the ring. These distortions result in a strong perturbation of the resonance delocalization, and subsequently in both a loss of planarity and a weakening of several bonds within the ring. Accordingly, a low activation barrier (22 kJ mol^{-1}) is obtained for the cleavage of C–N bond, which leads to the intermediate **F**, which may expel HNCO through the **TS6** transition state. It is worth noting that all attempts to find a way in which structure **4** can be connected to the intermediate **F**, in particular a kind of retro-Diels–Alder rearrangement, failed. Note also that like for Pb^{2+} ions [34], the most favorable path for the loss of HNCO results in a complex in which the metallic center interacts with an acyclic fragment that can be described as a ketene bearing an imino group.

The C2–N1 bond cleavage in structure **5b** is energetically much more demanding, with an activation barrier of 293 kJ mol^{-1}, connecting this local minimum with the **G** intermediate, which further dissociates by losing HOCN. Although the loss of HNCO arising from structure **8** is the most favorable processes, the elimination of HOCN from **5b** cannot be ruled out and therefore the neutral molecule generated together with the *m*/*z* 54.50 ion, could be either HNCO or HOCN.

Elimination of water is the other neutral loss observed onto the MS/MS spectra. Since uracil contains two oxygen atoms at positions 2 and 4, this H_2O molecule can, in principle contain, any of these two oxygen atoms. Obviously, the most suitable structures for water loss are the enolic forms **2b** and **5b**, because this reduces the required hydrogen transfers to only one. However, for the global minimum **2b**, this 1,3-H transfer is thermodynamically not favored (401 kJ mol^{-1}) and therefore appears very unlikely since the corresponding dissociation limit lies 2 kJ mol^{-1} higher in energy than the entrance channel. The process involving the enolic form **5b** is, conversely, much more favorable, since the hydrogen transfer from N1H towards the O2 center leading to the minimum **H** is associated with an activation barrier of 273 kJ mol^{-1}. Dissociation of **H** results in an exit channel located well below the entrance channel (see Fig. 4).

3.2.3. Ca^{2+}–uracil vs. Cu^{2+}–uracil, Pb^{2+}–uracil, M^+–uracil (M = H, Li, Na, K) fragmentations

Interaction of uracil with metal ions, as pointed out in the introduction, may provide interesting information on the behavior of this molecule in biological media, and how this behavior may depend on the nature of the metal ion. The same can be said as far as protonated uracil is concerned. Since both experimental and theoretical information are available for the uracil/Pb^{2+}, uracil/Cu^{2+} uracil/M^+ (M = Li, Na, K) and uracil/H^+ systems, we thought that it would be interesting to compare the chemistry of Ca^{2+} to those of Cu^{2+}, Pb^{2+}, alkali metal ions and proton. When Ca^{2+} is compared to Cu^{2+} or Pb^{2+}, the first significant difference is the nature of the metal ion–uracil interaction. As illustrated in Fig. 5, for the adducts formed by the direct interaction of the metal with neutral uracil in its equilibrium conformation, while the association of Ca^{2+} is essentially electrostatic, the binding of Cu^{2+} exhibits a non-negligible covalent character, and the interaction with Pb^{2+} could be considered as significantly covalent.

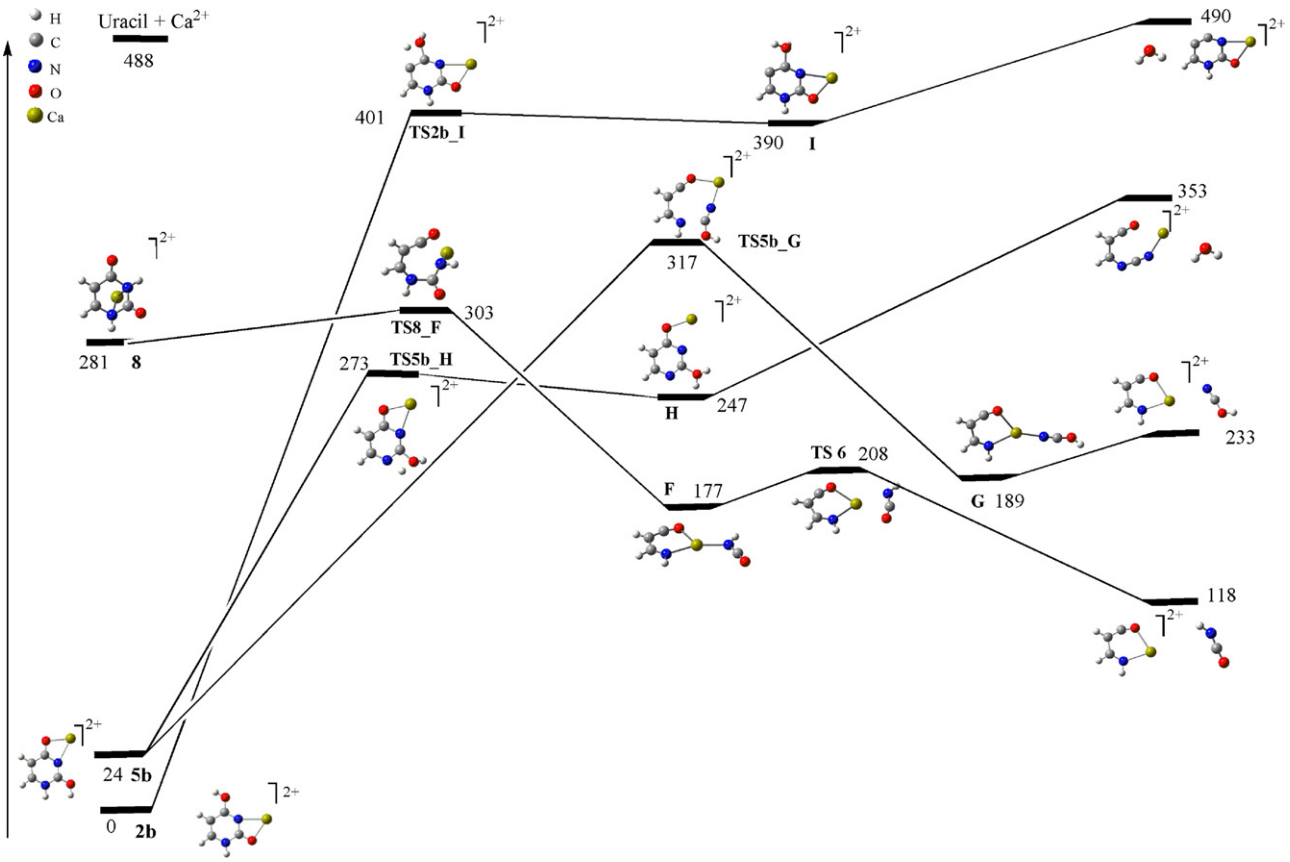

Fig. 4. Potential energy profile corresponding to the loss of [H,N,C,O] and H_2O with origin in the local minima **4**, **5b** and the global minimum **2b**. Relative energies are in kJ mol^{-1}.

Indeed, while the energy density between the metal and the organic moiety is positive in the case of Ca^{2+} complexes as typically observed for electrostatic interactions, it is found negative for the Cu^{2+} and Pb^{2+} analogues, indicating that in these latter cases the covalent character of the interaction is not at all negligible. The greater overlap between the valence shell of Pb and that of the oxygen atom in uracil clearly shows that this covalency is particularly large in $[Pb(uracil)]^{2+}$ complexes. As it has been discussed previously in the literature [26], Cu^{2+} has an oxidant character which Ca^{2+} does not have. This is a consequence of two concomitant factors, on one hand the large difference between the recombination energy for these dications (20.29 eV for Cu^{2+} and 15.03 eV for Pb^{2+} but only 12.03 eV for Ca^{2+}) [49], and on the other hand the fact that Cu^{2+} has low-lying empty d orbitals, able to easily accommodate electronic charge from the base, whereas the 4s empty orbital of Ca^{2+} lies very high in energy. The situation is rather similar in Pb^{2+}, where again low-lying empty p orbitals are available for the charge transfer from the base. The fact that the charge transfer easily occurs between the base and Cu^{2+} and Pb^{2+} is nicely mirrored, as mentioned above, in the energy density

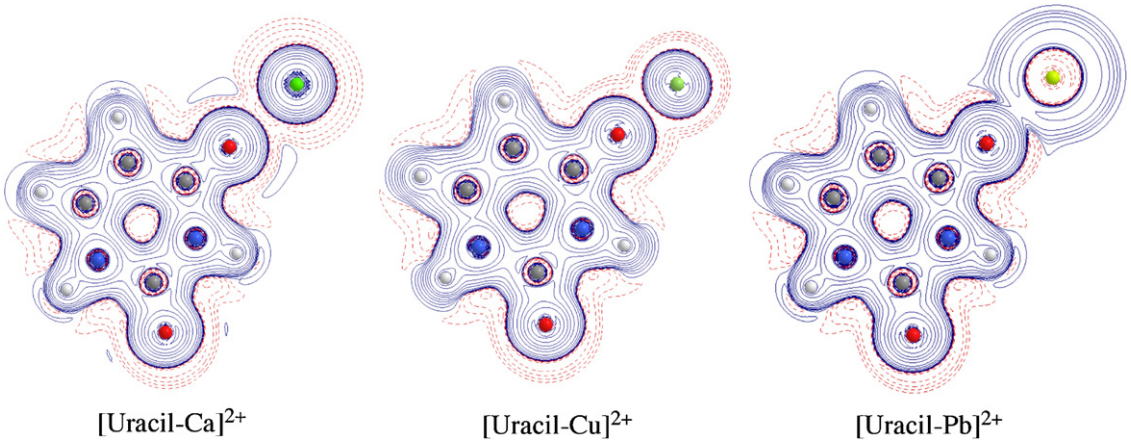

Fig. 5. Energy density plot for the most stable adducts formed by association of Ca^{2+}, Cu^{2+} and Pb^{2+} to uracil. Solid blue and dashed red lines correspond to negative and positive values of the energy density, respectively.

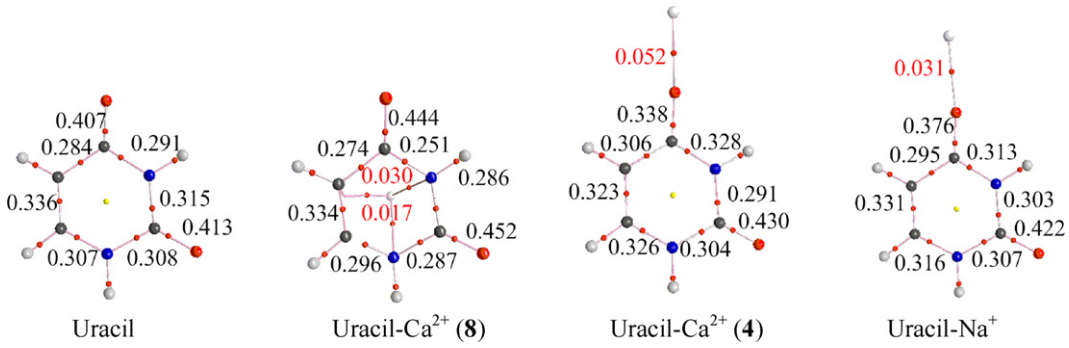

Fig. 6. Molecular graphs for uracil and its Ca^{2+} complexes in which the metal ion is bridging between the two N atoms (**8**) or attached to O4 (**4**). The molecular graph of complex **4** when the metal ion is Na^+ is also included for the sake of comparison. Red dots denote bond critical points. Electron densities are in a.u. (For interpretation of the references to color in text, the reader is referred to the web version of the article.)

maps, which shows that for Ca^{2+} the interaction is typically the one between two closed systems, and therefore, essentially electrostatic, while for Cu^{2+} and Pb^{2+} there is a non-negligible charge exchange between the interacting subunits. The main consequence of these dissimilarities is that in $[Cu(uracil)]^{2+}$ and $[Pb(uracil)]^{2+}$ complexes the charge transfer from the base towards the metal ion is quite large resulting in a significant acidity enhancement of the uracil moiety [32], which strongly favors a proton transfer processes within $[M(uracil)_n]^{2+}$ ($n \geq 2$, M = Pb) clusters from one uracil ligand to another. In fact this intracluster proton transfer would be consistent with the fact that for this systems both $[M(uracil)–H]^+$ and $[uracil]H^+$ monocations are detected. This is not the case for the $[Ca(uracil)]^{2+}$ complex, because the charge transfer from the base to the metal ion, as indicated above, is very small. Hence, whereas $[Ca(uracil)]^{2+}$ ions are observable in the gas phase under our electrospray conditions, $[Cu(uracil)]^{2+}$ and $[Pb(uracil)]^{2+}$ species are not, and only $[M(uracil)–H]^+$ (M = Cu, Pb) complexes, likely originating through proton transfer processes within $[M(uracil)_n]^{2+}$ ($n \geq 2$, M = Pb) clusters as indicated above, have been detected [34,35]. The fact that the aforementioned intra-cluster proton transfer is favored in $[M(uracil)_n]^{2+}$ ($n \geq 2$, M = Cu, Pb) is also consistent with the exothermicity of the $[Cu(uracil)]^{2+} \rightarrow [Cu(uracil)–H]^+ + H^+$ Coulomb explosion, whereas the similar process for Ca containing systems is endothermic [24]. Hence, for Cu^{2+} and Pb^{2+} interactions the smallest complexes which undergo fragmentation are the $[Cu(uracil)–H]^+$ or $[Pb(uracil)–H]^+$ singly charged species [70]. One of the consequences of this fact is that $CuOH^+$ and $PbOH^+$ are not observed as products of their fragmentation, whereas for $[Ca(uracil)]^{2+}$ complexes $CaOH^+$ is the most abundant product. For similar reasons, the loss of NCO• radical is not observed for $[Ca(uracil)]^{2+}$, whereas for Cu, the fact that uracil is already deprotonated renders the loss of the NCO• radical possible. For Pb, the interaction with the basic sites of uracil has a much more covalent character and the formation of $[PbNCO]^+$ is observed instead of the elimination of NCO•.

On the other hand, elimination of [H,N,C,O] is observed with the three divalent metals. In all cases this loss is the second more important process, and the atoms involved in this dissociation are systematically the carbon C2, the oxygen attached to C2 and the nitrogen N3. In fact, the mechanism is rather similar for the three systems and implies a complex in which the metal simultaneously interacts with the two nitrogen atoms (structure **8**). Such a binding mode induces an activation of most of the bonds within the uracil ring reflected in a decrease of the electron density at the corresponding bond critical points, this decrease being particularly large for both the N3C4 and the N1C2 bonds (see Fig. 6), whereas the C4O bond becomes reinforced.

The most significant difference between the MS/MS spectra of the $[Ca(uracil)]^{2+}$ and protonated uracil ions is that a loss of NH_3 is only detected in the latter case. This likely reflects the easiness of a proton transfer within the protonated species towards one of the NH ring groups, which is not favorable in the $[Ca(uracil)]^{2+}$ complexes. Consistently with these arguments, NH_3 loss is observed neither in photoionization [63] nor in electron impact [64,65] mass spectrometry studies of uracil. In all cases however a loss of HNCO is observed. It is worth noting that the structure proposed for the ion corresponding to the loss of HNCO from photoionized uracil ($[O{=}C–CH{=}CH–NH]^+$) is in agreement with the structure of the corresponding Ca^{2+} complex likely to be detected in our study, in which the metal dication bridges between the carbonyl oxygen atom and the NH imino group of the O=C–CH=CH–NH moiety (Fig. 4).

The differences in the collision-induced unimolecular reactivity between $[Ca(uracil)]^{2+}$ and $[M(uracil)]^+$ ions, where M is an alkali metal are also significant since the only fragmentation observed for $[uracil–alkali]^+$ complexes is the loss of the nucleobase [2]. This likely reflects the fact that the polarization of the electron density of the base is significantly larger in the presence of the dication, and therefore some of the bonds of uracil become significantly activated and finally cleaved, whereas the activation induced by the interaction with alkali monocations is rather weak and therefore not sufficient to promote a bond fission. This is actually reflected in the corresponding molecular graphs, which show indeed that the activation or reinforcement of the uracil-moiety bonds are stronger upon Ca^{2+} than upon Na^+ association. As illustrated in Fig. 6, the activation of the C=O bond induced by Ca^{2+} is significantly larger than the one induced by Na^+, mirrored in a much larger decrease of the electron density at the corresponding bond critical point. This also applies for the activation of the C2N3 and the C5C6 bonds or with respect to the reinforcement of the N3C4 and C4C5 linkages. In agreement with the experimental results, the bond between the metal and the basic site of uracil is much weaker for Na^+ than for Ca^{2+}.

4. Conclusions

The investigation of the gas-phase interactions between Ca^{2+} and uracil by means of nanoelectrospray ionization/mass spectrometry techniques shows that charge separation processes leading to singly-charged species dominate in the MS/MS spectra of $[Ca(uracil)]^{2+}$ ions. Actually, the most intense peaks correspond to $[CaOH]^+$ (m/z 56.97) and $[C_4,N_2,O,H_3]^+$ (m/z 95.03) Nevertheless, additional product ions corresponding to the loss of neutral species such as [H,N,C,O] and H_2O have been also detected. A systematic study of the CID spectra obtained with different labeled

species concludes unambiguously that the loss of [H,N,C,O] involves exclusively atoms C2 and N3.

A DFT study of the energy profile associated with the various processes shows that the aforementioned charge separation process may indifferently involves three different structures, namely **2b**, **1** and **4**, and that the three proposed mechanisms are thermodynamically allowed and roughly equally probable. Hence, the formation of $[CaOH]^+$ may be accompanied with the generation of three different $[C_4,N_2,O,H_3]^+$ isomers, two cyclic ones and one (the most stable) with an aliphatic open-chain structure.

The loss of [H,N,C,O] arises from complexes **8** and **5b**, the neutrals expelled in both processes being different. While the most favorable pathway (originating from structure **8**) leads to the loss of isocyanic acid H–N=C=O, **5b** leads to the elimination of HOCN.

Comparison between Ca^{2+}/uracil, Cu^{2+}/uracil and Pb^{2+}/uracil systems denotes the existence of both significant differences and interesting similarities. Whereas the most favorable process upon collision for the $[Ca(uracil)]^{2+}$ complex is a Coulomb explosion yielding $CaOH^+$, $CuOH^+$ or $PbOH^+$ are practically not detected for $[Pb(uracil)–H]^+$ or $[Cu(uracil)–H]^+$ complexes. It is also worth reminding that doubly charged $[M(uracil)]^{2+}$ ions were not detected for copper and lead. Similarly, in the fragmentation of the $[Ca(uracil)]^{2+}$ complex the loss of $NCO^•$ is not observed while this is one of the reaction channels for Cu or Pb, although for Pb the NCO fragment appears associated with the singly-charged metal. Conversely, the elimination of HNCO is observed for the three systems, and in all cases implies the C2, O2 and N3 atoms.

Unlike protonated uracil, elimination of ammonia is not observed with calcium. Finally, while the unimolecular reactivity upon collision of the $[Ca(uracil)]^{2+}$ complex is quiet rich, that of $[uracil–alkali]^+$ complexes only shows the elimination of uracil.

Acknowledgments

This work has been partially supported by the DGI Project No. CTQ2009-13129-C02, by the Project MADRISOLAR2, Ref.: S2009PPQ/1533 of the Comunidad Autónoma de Madrid, by Consolider on Molecular Nanoscience CSD2007-00010, and by the COST Action COST CM0702. A generous allocation of computing time at the CCC of the UAM is also acknowledged. JYS would like to thank Denis Brasseur (Sanofi-Aventis) for kindly providing few milligrams of uracil-3-^{15}N.

Appendix A. Supplementary data

Supplementary data associated with this article can be found, in the online version, at doi:10.1016/j.ijms.2011.05.018.

References

[1] B.A. Cerda, C. Wesdemiotis, J. Am. Chem. Soc. 118 (1996) 11884.
[2] M.T. Rodgers, P.B. Armentrout, J. Am. Chem. Soc. 122 (2000) 8548.
[3] J.D. Gu, J. Leszczynski, J. Phys. Chem. A 105 (2001) 10366.
[4] N. Russo, M. Toscano, A. Grand, J. Am. Chem. Soc. 123 (2001) 10272.
[5] N. Russo, M. Toscano, A. Grand, J. Phys. Chem. B 105 (2001) 4735.
[6] A. Kufelnicki, I. Kupinska, J. Jezierska, J. Ochocki, Pol. J. Chem. 76 (2002) 1559.
[7] N. Russo, E. Sicilia, M. Toscano, A. Grand, Int. J. Quantum Chem. 90 (2002) 903.
[8] Z.B. Yang, M.T. Rodgers, Int. J. Mass Spectrom. 241 (2005) 225.
[9] M. Kabelac, P. Hobza, J. Phys. Chem. B 110 (2006) 14515.
[10] Z.B. Yang, M.T. Rodgers, J. Phys. Chem. A 110 (2006) 1455.
[11] E. Rincon, M. Yáñez, A. Toro-Labbe, O. Mó, Phys. Chem. Chem. Phys. 9 (2007) 2531.
[12] E.A.L. Gillis, K. Rajabi, T.D. Fridgen, J. Phys. Chem. A 113 (2009) 824.
[13] E.A.L. Gillis, T.D. Fridgen, Int. J. Mass Spectrom. 297 (2010) 2.
[14] E.L. Zins, C. Pepe, D. Schroder, J. Mass Spectrom. 45 (2010) 740.
[15] J.V. Burda, J. Sponer, J. Leszczynski, P. Hobza, J. Phys. Chem. B 101 (1997) 9670.
[16] J. Sponer, M. Sabat, J.V. Burda, J. Leszczynski, P. Hobza, J. Phys. Chem. B 103 (1999) 2528.
[17] N. Russo, M. Toscano, A. Grand, J. Phys. Chem. A 107 (2003) 11533.
[18] T. Marino, M. Toscano, N. Russo, A. Grand, Int. J. Quantum Chem. 98 (2004) 347.
[19] M. Franska, Eur. J. Mass Spectrom. 13 (2007) 339.
[20] E.L. Zins, S. Rochut, C. Pepe, J. Mass Spectrom. 44 (2009) 40.
[21] E.L. Zins, S. Rochut, C. Pepe, J. Mass Spectrom. 44 (2009) 813.
[22] N. Russo, M. Toscano, A. Grand, J. Mass Spectrom. 38 (2003) 265.
[23] T. Marino, D. Mazzuca, N. Russo, M. Toscano, A. Grand, Int. J. Quantum Chem. 110 (2010) 138.
[24] A. Lamsabhi, M. Yáñez, J.-Y. Salpin, J. Tortajada, Gas Phase Chemistry of Organocopper Compounds, John Wiley & Sons, Chichester, 2009.
[25] I. Corral, O. Mó, M. Yáñez, J.Y. Salpin, J. Tortajada, L. Radom, J. Phys. Chem. A 108 (2004) 10080.
[26] C. Trujillo, A.M. Lamsabhi, O. Mó, M. Yáñez, Phys. Chem. Chem. Phys. 10 (2008) 3229.
[27] C. Trujillo, O. Mó, M. Yáñez, J.-Y. Salpin, J. Tortajada, ChemPhysChem 8 (2007) 1330.
[28] C. Trujillo, O. Mó, M. Yáñez, J. Tortajada, J.Y. Salpin, J. Phys. Chem. B 112 (2008) 5479.
[29] I. Corral, O. Mó, M. Yáñez, J.Y. Salpin, J. Tortajada, D. Moran, L. Radom, Chem. Eur. J. 12 (2006) 6787.
[30] I. Corral, C. Trujillo, J.Y. Salpin, M. Yáñez, Kinetics and Dynamics: from Nano- to Bio-Scale, Springer, 2010.
[31] A.M. Lamsabhi, M. Alcamí, O. Mó, M. Yáñez, J. Tortajada, ChemPhysChem 5 (2004) 1871.
[32] A.M. Lamsabhi, M. Alcamí, O. Mó, M. Yáñez, J. Tortajada, J. Phys. Chem. A 110 (2006) 1943.
[33] A.M. Lamsabhi, M. Alcamí, O. Mó, M. Yáñez, J. Tortajada, J.Y. Salpin, ChemPhysChem 8 (2007) 181.
[34] S. Guillaumont, J. Tortajada, J.Y. Salpin, A.M. Lamsabhi, Int. J. Mass Spectrom. 243 (2005) 279.
[35] C. Gutle, J.Y. Salpin, T. Cartailler, J. Tortajada, M.P. Gaigeot, J. Phys. Chem. A 110 (2006) 11684.
[36] W.R. Farkas, Biochim. Biophys. Acta 155 (1968) 401.
[37] M. Ferreira-Cravo, J. Ventura-Lima, J.Z. Sandrini, L.L. Amado, L.A. Geracitano, M. Rebelo, A. Bianchini, J.M. Monserrat, Ecotoxicol. Environ. Saf. 72 (2008) 388.
[38] E.J. Land, C.A. Ramsden, P.A. Riley, M.R.L. Stratford, Tohoku J. Exp. Med. 216 (2008) 231.
[39] D. Ozcelik, H. Uzun, Biol. Trace Elem. Res. 127 (2009) 45.
[40] R.A. Goyer, Handbook on Toxicity of Inorganic Compounds, Dekker, New York, 1988.
[41] M.J. Frisch, G.W. Trucks, H.B. Schlegel, G.E. Scuseria, M.A. Robb, J.R. Cheeseman, V.G. Zakrzewski, J.A.J. Montgomery, R.E. Stratmann, J.C. Burant, S. Dapprich, J.M. Millam, A.D. Daniels, K.N. Kudin, M.C. Strain, O. Farkas, J. Tomasi, V. Barone, M. Cossi, R. Cammi, B. Mennucci, C. Pomelli, C. Adamo, S. Clifford, J. Ochterski, G.A. Petersson, P.Y. Ayala, Q. Cui, K. Morokuma, D.K. Malick, A.D. Rabuck, K. Raghavachari, J.B. Foresman, J. Cioslowski, J.V. Ortiz, B.B. Stefanov, G. Liu, A. Liashenko, P. Piskorz, I. Komaromi, R. Gomperts, R.L. Martin, D.J. Fox, T. Keith, M.A. Al-Laham, C.Y. Peng, A. Nanayakkara, C. Gonzalez, M. Challacombe, P.M.W. Gill, B. Johnson, W. Chen, M.W. Wong, J.L. Andres, M. Head-Gordon, E.S. Replogle, J.A. Pople, Gaussian03. Revised E1, Gaussian, Inc, 2004.
[42] C. Lee, W. Yang, R.G. Parr, Phys. Rev. B 37 (1988) 785.
[43] A.D. Becke, J. Chem. Phys. 98 (1993) 5648.
[44] I. Corral, O. Mó, M. Yáñez, A.P. Scott, L. Radom, J. Phys. Chem. A 107 (2003) 10456.
[45] A.P. Scott, L. Radom, J. Phys. Chem. 100 (1996) 16502.
[46] R.F.W. Bader, Atoms in Molecules: A Quantum Theory, Clarendon Press Oxford Univ., Oxford, 1990.
[47] C.F. Matta, R.J. Boyd, The Quantum Theory of Atoms in Molecules, Wiley-VCH Verlag GmbH & Co., KGaA, Weinheim, 2007.
[48] T.A. Keith, AIMAll (aim.tkgristmill.com), version 10.03.25, 2010.
[49] The National Institute of Standards and Technology (NIST), http://webbook.nist.gov/chemistry/.
[50] A.T. Blades, P. Jayaweera, M.G. Ikonomou, P. Kebarle, Int. J. Mass Spectrom. Ion Processes 102 (1990) 251.
[51] A.T. Blades, P. Jayaweera, M.G. Ikonomou, P. Kebarle, J. Chem. Phys. 92 (1990) 5900.
[52] M. Kohler, J.A. Leary, J. Am. Soc. Mass Spectrom. 8 (1997) 1124.
[53] S.E. Rodriguez-Cruz, R.A. Jockusch, E.R. Williams, J. Am. Chem. Soc. 120 (1998) 5842.
[54] M. Peschke, A.T. Blades, P. Kebarle, J. Phys. Chem. A 102 (1998) 9978.
[55] S.E. Rodriguez-Cruz, R.A. Jockusch, E.R. Williams, J. Am. Chem. Soc. 121 (1999) 8898.
[56] M. Beyer, E.R. Williams, V.E. Bondybey, J. Am. Chem. Soc. 121 (1999) 1565.
[57] A.A. Shvartsburg, J.G. Wilkes, J.O. Lay, K.W. Michael Siu, Chem. Phys. Lett. 350 (2001) 216.
[58] A.A. Shvartsburg, K.W.M. Siu, J. Am. Chem. Soc. 123 (2001) 10071.
[59] A.A. Shvartsburg, J.G. Wilkes, J. Phys. Chem. A 106 (2002) 4543.
[60] A.A. Shvartsburg, Chem. Phys. Lett. 376 (2003) 6.
[61] C.C. Nelson, J.A. McCloskey, J. Am. Soc. Mass Spectrom. 5 (1994) 339.
[62] H.C. Liu, J.L. Sun, Y.H. Hu, K.L. Han, S.H. Yang, Chem. Phys. Lett. 389 (2004) 342.
[63] H.-W. Jochims, M. Schwell, H. Baumgartel, S. Leach, Chem. Phys. 314 (2005) 263.
[64] J.M. Rice, G.O. Dudek, M. Barber, J. Am. Chem. Soc. 87 (1965) 4569.

[65] S.M. Hecht, A.S. Gupta, N.J. Leonard, Biochim. Biophys. Acta 182 (1969) 444.
[66] B. Coupier, B. Farizon, M. Farizon, M.J. Gaillard, F. Gobet, N.V.D. Faria, G. Jalbert, S. Ouaskit, M. Carre, B. Gstir, G. Hanel, S. Denifl, L. Feketeova, P. Scheier, T.D. Mark, Eur. Phys. J. D 20 (2002) 459.
[67] C. Trujillo, A.M. Lamsabhi, O. Mó, M. Yáñez, J.Y. Salpin, Org. Biol. Chem. 6 (2008) 3695.
[68] A.M. Lamsabhi, M. Alcamí, O. Mó, M. Yáñez, ChemPhysChem 4 (2003) 1011.
[69] M. Kurinovich, J. Lee, J. Am. Chem. Soc. 122 (2000) 6258.
[70] Note: However, that $CuOH^+$ and $PbOH^+$ ions are indeed detected in the corresponding source spectra obtained in electrospray experiments involving uracil and Cu^{2+} or Pb^{2+}, respectively.